Downloaded from orbit.dtu.dk on: May 05, 2023

DTU Library

Ear-to-Ear Propagation Model based on Geometrical Theory of Diffraction

Kammersgaard, Nikolaj Peter Brunvoll; Kvist, Søren H.; Thaysen, Jesper; Jakobsen, Kaj Bjarne

Published in:
IEEE Transactions on Antennas and Propagation

Link to article, DOI:
10.1109/TAP.2018.2882587

Publication date:
2019

Document Version
Peer reviewed version

Link back to DTU Orbit

Citation (APA):
Kammersgaard, N. P. B., Kvist, S. H., Thaysen, J., & Jakobsen, K. B. (2019). Ear-to-Ear Propagation Model based on Geometrical Theory of Diffraction. *IEEE Transactions on Antennas and Propagation*, *67*(2), 1153-1160. https://doi.org/10.1109/TAP.2018.2882587

General rights
Copyright and moral rights for the publications made accessible in the public portal are retained by the authors and/or other copyright owners and it is a condition of accessing publications that users recognise and abide by the legal requirements associated with these rights.

- Users may download and print one copy of any publication from the public portal for the purpose of private study or research.
- You may not further distribute the material or use it for any profit-making activity or commercial gain
- You may freely distribute the URL identifying the publication in the public portal

If you believe that this document breaches copyright please contact us providing details, and we will remove access to the work immediately and investigate your claim.

This article has been accepted for publication in a future issue of this journal, but has not been fully edited. Content may change prior to final publication. Citation information: DOI 10.1109/TAP.2018.2882587, IEEE Transactions on Antennas and Propagation

Ear-to-Ear Propagation Model based on Geometrical Theory of Diffraction

Nikolaj P. B. Kammersgaard, Søren H. Kvist, Jesper Thaysen, and Kaj B. Jakobsen

***Abstract*—An ear-to-ear propagation model based on geometrical theory of diffraction is presented. The model uses the creeping wave loss along the geodesic paths that connect the ears. It is the first model to investigate which geodesic paths that link the ears. The model uses geometrical theory of diffraction expressions for a lossy dielectric material, which is a much better approximation of the human body than the perfect electric conductor approximation often used. The model is validated for the industrial, scientific and medical band at 2.45 GHz. The model is valid at any frequency range as long as the propagation loss through the head is significantly higher than the propagation loss around the head. Likewise, the model could be used for other areas of the body. The comparison with simulations show strong correlation. The antenna orientation and frequency sweeps were preformed to further investigate the model. The sweeps change the radiation pattern of the antenna to utilize different paths around the head, but the model still correlates with the simulation. This validates the models division of the ear-to-ear propagation into different geodesic paths around the head.**

***Index Terms*—Geometrical Theory of Diffraction, On-Body, Off-Body, WBAN, Ear-to-Ear, Hearing Instruments, Creeping Wave.**

I. Introduction

BODY-worn antennas and the area of on-body propagation have been a major research area in recent years. The continuous decrease in size and power consumption in modern electronics, together with improved receiver sensitivity, has enabled the implementation of wireless communication in more and more body-worn devices. Wireless communication is now a key part of for example smart watches, hearing instruments (HIs) and so-called 'truly' wireless headsets. In modern HIs, connectivity to off-body accessories and smart phones is becoming a must-have feature. The connectivity enables the HI user to receive phone calls, listen to music, or watch TV seamlessly. In most cases the Industrial, Scientific and Medical (ISM) band at 2.45 GHz is used for several reasons. It is available world wide and license free. Also, the BlueTooth® protocol is located in this band and is implemented in virtually all smart phones.

Besides connectivity with off-body devices it is desirable to **achieve** ear-to-ear (E2E) connectivity between the HIs on either side of the head. The E2E communication between the HIs enables acoustic algorithms that improve the directionality of the sound amplification. It also improves the HIs' ability to coordinate and adjust the acoustic settings to the current acoustic environment. Furthermore, the E2E communication can be used to improve the range of the off-body communication [1].

In the recently emerged headset category of 'truly' wireless headsets, the E2E communication is also very important. The 'truly' refers to the fact that the headset consists of two separate devices in each ear that can only communicate with each other wirelessly. The E2E communication is crucial to the synchronization of the devices. Furthermore, in the current BlueTooth® protocol, streaming can only be done to one device. Therefore, the master of the two ear pieces needs to relay the received audio signal to the other device.

The many applications of the E2E channel illustrate the importance of a good understanding and modeling of the E2E propagation. Furthermore, the principles of the E2E channel are the same for other on-body propagation channels such as the pocket-to-ear channel between an audio streaming device in the pocket and a headset or HI in the ear. General on-body propagation models are numerous, for example [2]–[8]. Only a few models specific to the head exist [9], [10]. Many of these models use a perfect electric conductor (PEC) approximation of the human body [5]–[10], which is a rather crude model of the human body at 2.45 GHz, as discussed in [11]. Especially models of the head, but also many of the general models, do not clearly investigate or explain which paths the on-body propagation follows. In [10] two paths around the head are included, one around the front and one around the back. In [9] infinitely many paths are included. Many of the presented propagation models use geometrical theory of diffraction (GTD) as the approximation. It will also be applied here. In GTD it is well known that the propagation follows the geodesic lines on the surface of the object.

The purpose of this paper is to investigate the geodesic paths around the head that the on-body propagation follows. Combined with more exact approximations of the on-body propagation by a lossy dielectric GTD approximation [12], the on-body paths will be used to create a new E2E propagation model. The model will be the first to determine and make use of the geodesic lines on the head. At the same time it will be the first E2E model to use a lossy dielectric GTD approximation of the head instead of a PEC approximation.

In Section II the theoretical parts of the model will be presented. In Section III the simulation setup used to validate the model is described. The numerical challenges of implementing the model is discussed in Section IV. The results of the model as well as the simulations are presented and discussed in Section V. Finally, the conclusion is found in Section VI.

N. P. B. Kammersgaard and K. B. Jakobsen are with the Electromagnetic Systems Group, Department of Electrical Engineering, Technical University of Denmark, Kgs. Lyngby, 2800 Denmark (e-mail: npivka@elektro.dtu.dk).

N. P. B. Kammersgaard, S. H. Kvist and J. Thaysen are with GN Hearing A/S, Ballerup, 2750 Denmark.

Manuscript submitted January, 2018.

0018-926X (c) 2018 IEEE. Personal use is permitted, but republication/redistribution requires IEEE permission. See http://www.ieee.org/publications_standards/publications/rights/index.html for more information.

This article has been accepted for publication in a future issue of this journal, but has not been fully edited. Content may change prior to final publication. Citation information: DOI 10.1109/TAP.2018.2882587, IEEE Transactions on Antennas and Propagation

II. Ear-to-Ear On-Body Propagation Model

In [12] it was shown how to calculate the diffracted fields from a point source on any given lossy dielectric convex opaque structure. The diffracted fields from an electric point source $\vec{J}_{\mathrm{i}}$ on the surface of the structure along a given geodesic line are given by:

$$\vec{E}^{\mathrm{d}} \sim \frac{jk_0\eta_0}{4\pi}\vec{J}_{\mathrm{i}} \cdot \overline{\overline{V}} e^{-jk_0 t}\sqrt{\frac{\mathrm{d}\psi_0}{\mathrm{d}\chi}} \tag{1}$$

where $\eta_0 = \sqrt{\frac{\mu_0}{\epsilon_0}}$ is the intrinsic impedance of free space, μ_0 and ϵ_0 are the permeability and permittivity of free space, respectively, $k_0 = \omega\sqrt{\epsilon_0\mu_0}$ is the wavenumber of free space and ω the angular frequency, t is the distance from the source along the geodesic line, $\mathrm{d}\chi$ is the distance between adjacent rays at the observation point, $\mathrm{d}\psi_0$ is the angle between adjacent rays at the source, and

$$\overline{\overline{V}} \sim \sum_{p=1}^{\infty}\left(\hat{t}' L^{\mathrm{e}}_{p,\mathrm{t}} + \hat{b}' L^{\mathrm{e}}_{p,\mathrm{b}} + \hat{n}' L^{\mathrm{e}}_{p,\mathrm{n}}\right)\left(\hat{t} A^{\mathrm{e}}_{p,\mathrm{t}} + \hat{b} A^{\mathrm{e}}_{p,\mathrm{b}} + \hat{n} A^{\mathrm{e}}_{p,\mathrm{n}}\right) e^{-\int_0^t \alpha_p \mathrm{d}t} \tag{2}$$

where $(\hat{t}', \hat{n}', \hat{b}')$ are the tangential, normal, and binormal unit vectors at the source point, respectively, and equivalently $(\hat{t}, \hat{n}, \hat{b})$ are the unit vectors at the observation point. The $L^{\mathrm{e}}_{p,i}$ and $A^{\mathrm{e}}_{p,i}$ are launching and attachment coefficients for electric point sources of specific polarizations, and α_p is the attenuation of the creeping wave. Exact expressions are found in [12], but the coefficients depend on frequency, constitutive parameters, and geometric factors. The subscript p refers to different modes, but in the deep shadow the first mode is all dominant and the summation over p will not be done in the remainder of the paper. Instead only the first mode will be used. Furthermore, the tangential and binormal contribution will be ignored since the magnitude of the launching and attachment coefficients for the first mode on the human body are more than $20\,\mathrm{dB}$ lower than the normal.

The electric field transmitted by an antenna in the polarization normal to the surface of the body of interest, $E^{\hat{n}}_{\mathrm{T}}$, can be expressed through the gain, G_{T}, and the transmit power, P_{T}, as:

$$E^{\hat{n}}_{\mathrm{T}} = \sqrt{\frac{2\eta_0 P_{\mathrm{T}} G^{\hat{n}}_{\mathrm{T}}}{4\pi}} e^{j\angle E^{\hat{n}}_{\mathrm{T}}} \frac{e^{-jk_0 r}}{r} \tag{3}$$

where r is the distance from the antenna. Note that the angle of the electric field transmitted by an antenna, $\angle E^{\hat{n}}_{\mathrm{T}}$ is only meaningful when the polarization is given. The transmitted electric field multiplied by $re^{jk_0 r}$ will take the place of the term $\frac{jk_0\eta_0}{4\pi}$ in Equation 1. This makes sense since the term $\frac{jk_0\eta_0}{4\pi}$ is exactly the magnitude of the electric fields radiated from a unit strength electric dipole source. For convenience, the reference to the normal component, $\hat{n}$, will be suppressed throughout the rest of the paper, e.g., E_{T} and E_{R}.

The received electric field normal to the surface, E_{R}, can then be calculated for a geodesic path:

$$E_{\mathrm{R}} = \sqrt{\frac{2\eta_0 P_{\mathrm{T}} G_{\mathrm{T}}}{4\pi}} e^{j\angle E_{\mathrm{T}}} L A e^{-jk_0 t - \int_0^t \alpha \mathrm{d}t}\sqrt{\frac{d\psi_0}{d\chi}} \tag{4}$$

By adding all the contributions from each of the geodesic paths that connect the transmitting and receiving antennas, the total open-circuit voltage at the terminals of the receiving antenna can be found:

$$V_{\mathrm{OC}} = \sum_{i=1}^{N} E_{\mathrm{R},i}\ell_{\mathrm{e},i} \tag{5}$$

where N is the total number of geodesic paths that connect the transmitting and receiving antennas and ℓ_{e} is the electrical length of the receiving antenna assuming perfect match given by:

$$\ell_{\mathrm{e}} = \sqrt{\frac{G_{\mathrm{R}}\lambda_0^2 R_{\mathrm{ant}}}{\pi\eta_0}} e^{j\angle E_{\mathrm{R}}} \tag{6}$$

where λ_0 is the free space wave length and R_{ant} is the resistive part of the antenna **input** impedance.

The received power can be calculated as:

$$P_{\mathrm{R}} = \frac{|V_{\mathrm{OC}}|^2}{8R_{\mathrm{ant}}} \tag{7}$$

By combining Equations 4, 5 and 7 the E2E path gain can be expressed as:

$$\frac{P_{\mathrm{R}}}{P_{\mathrm{T}}} = \left(\frac{\lambda_0}{4\pi}\right)^2 \left|\sum_{i=1}^{N}\sqrt{G_{\mathrm{R},i}G_{\mathrm{T},i}\frac{\mathrm{d}\psi_{0,i}}{\mathrm{d}\chi_i}} L_i A_i e^{j\left(\angle E_{\mathrm{R},i} + \angle E_{\mathrm{T},i}\right) - jk_0 t_i - \int_0^{t_i}\alpha_i \mathrm{d}t}\right|^2 \tag{8}$$

III. Simulation Setup

The model was validated by the use of Ansys HFSS 18.2 simulations. The on-body radiation patterns were exported from the simulations for use in the model. **The gain along the surface of the head in the directions of the different geodesics from the on-body radiations patterns are used as the gains, $G_{\mathrm{R},i}$ and $G_{\mathrm{T},i}$.** The simulations were run with extremely strict convergence criteria to ensure correct results. The main convergence criterion was that the maximum achievable path gain (MAPG) should not change more than 0.1 dB, equivalent to a change of 2.27%. The MAPG $|S^{\max}_{21}|$ is used to avoid the impact of the impedance match. It is the path gain $|S_{21}|$ obtained when both antennas are perfectly matched and can be calculated using [13]. Since the path gain $|S_{21}|$ is very low, the antenna matching on one side does not impact the antenna impedance on the other side in practice. Therefore, the MAPG $|S^{\max}_{21}|$ can be approximated by:

$$|S^{\max}_{21}| \approx \frac{|S_{21}|^2}{\left(1-|S_{11}|^2\right)\left(1-|S_{22}|^2\right)}. \tag{9}$$

For the reflection coefficient the convergence criterion was an absolute change of 0.02. Four consecutive converged passes were required before the simulation was considered converged.

The simulations were done on an Ansys HFSS version (faceted) of the Specific Anthropomorphic Mannequin (SAM), which had been modified with realistic ears, neck and shoulders. The neck and shoulders were included to ensure that no energy could creep around the bottom of the head. The

0018-926X (c) 2018 IEEE. Personal use is permitted, but republication/redistribution requires IEEE permission. See http://www.ieee.org/publications_standards/publications/rights/index.html for more information.

This article has been accepted for publication in a future issue of this journal, but has not been fully edited. Content may change prior to final publication. Citation information: DOI 10.1109/TAP.2018.2882587, IEEE Transactions on Antennas and Propagation

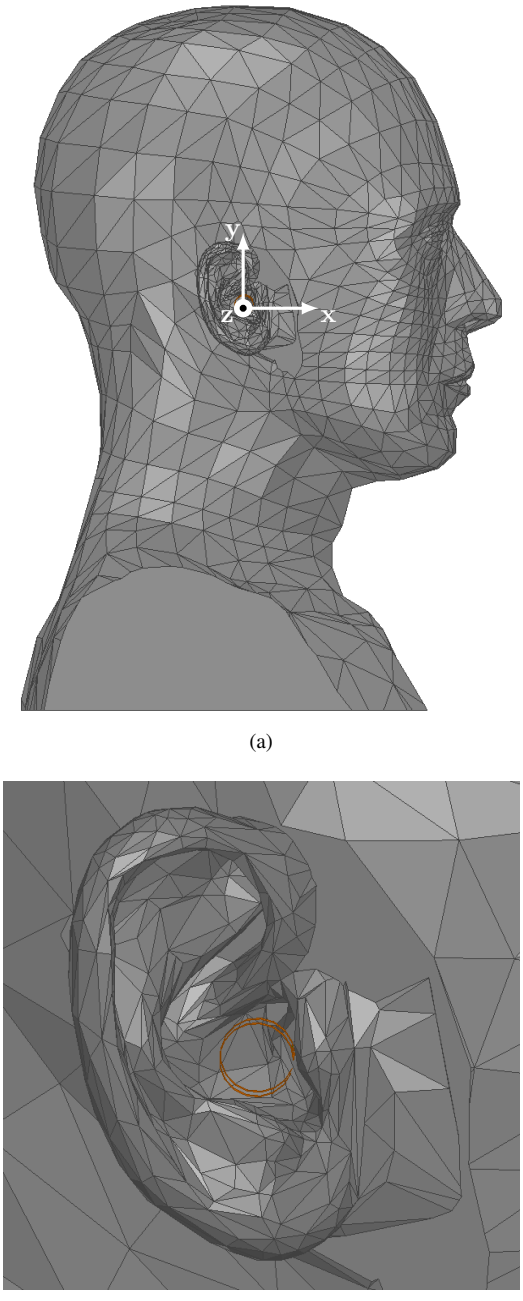

(a)

(b)

Fig. 1. The SAM phantom head (a) with the coordinate system used and a close up of the realistic ear (b) where the antenna can be seen (in red).

simulation model is seen in Fig. 1. The antenna simulated has been presented in detail in [14], where the simulation results were also validated against measurements. The antenna is visible in Fig. 1b. The simulations were all done at 2.45 GHz or for a frequency range with 2.45 GHz in the middle of the band. Therefore, the constitutive parameters used to model the human body were $\epsilon_r = 39.2$ and $\sigma = 1.8\,\mathrm{S/m}$ as specified in [15] as standard parameters for the human body. **With the orientation of the coordinate system shown in Fig. 1a, the XY-plane is the relevant to consider for the gains to use in 8.**

To investigate if the energy propagating through the head

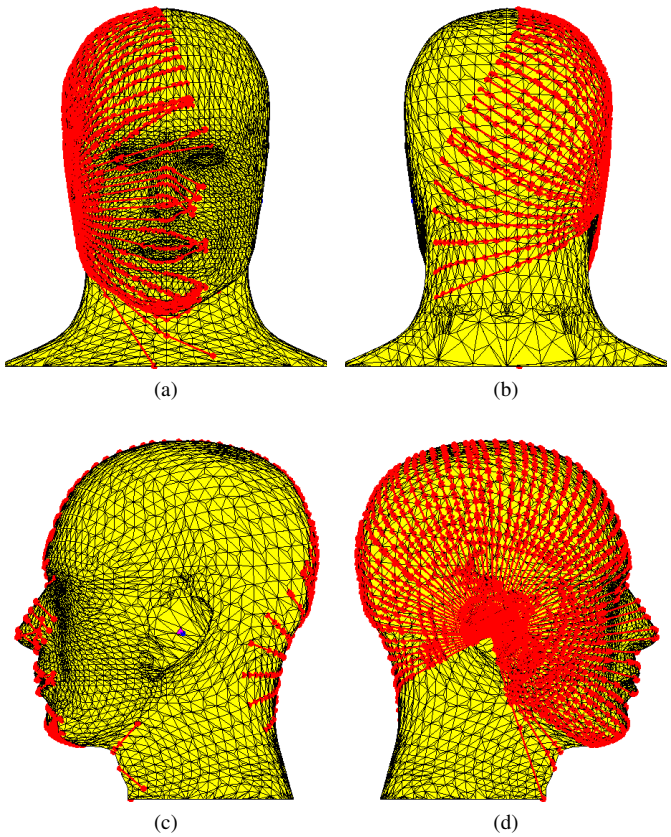

(a) (b) (c) (d)

Fig. 2. The SAM phantom head with the geodesic path originating from the position of the right ear seen from the front (a), back (b), left (c), and right (d) side of the head. The geodesic paths shown end at 200 mm.

has significant importance for the results, a simulation with absorbers all around the head was run. It was found that the MAPG becomes $-103.6\,\mathrm{dB}$ which is well below the $-78.3\,\mathrm{dB}$ of the equivalent simulation without absorbers. However, the level is enough to cause a variation of up to $\pm 0.5\,\mathrm{dB}$ dependent on the phase.

IV. Model Implementation

The main challenging part of implementing the proposed model is finding the geodesic lines on the given object, in this case the head. The geodesic lines are sometimes referred to as the shortest paths, although this can be a bit misleading. It is the generalization of straight lines to the surface of 3D objects. On a sphere the geodesic lines are the great circles, and on a cylinder they are helices. The formal definition is, that geodesic lines are lines on the surface that in their unit-speed parametrization only have acceleration perpendicular to the surface [16].

Here the geodesic lines were found on the head used for the simulations. The head is faceted to reduce the mesh complexity in Ansys HFSS. Therefore, the computation of the geodesic lines is very simple. On a facet, the geodesic line is naturally a straight line. When a geodesic line crosses from one facet to the next, the angle between the geodesic line and the edge separating the facets needs to stay constant. If one imagines

0018-926X (c) 2018 IEEE. Personal use is permitted, but republication/redistribution requires IEEE permission. See http://www.ieee.org/publications_standards/publications/rights/index.html for more information.

This article has been accepted for publication in a future issue of this journal, but has not been fully edited. Content may change prior to final publication. Citation information: DOI 10.1109/TAP.2018.2882587, IEEE Transactions on Antennas and Propagation

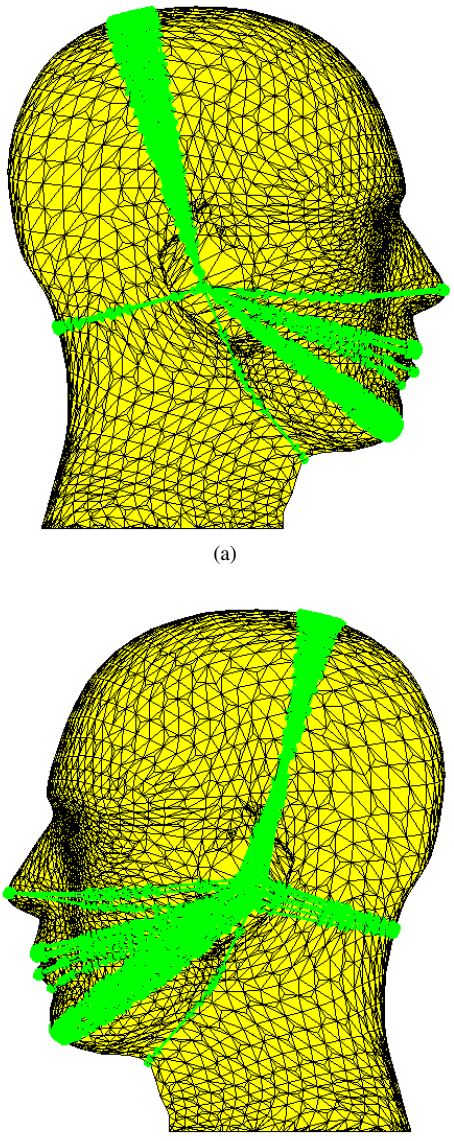

Fig. 3. The SAM phantom head geodesic lines that are emitted from the right ear and reaches the left ear seen from the right (a) and left (b) side of the head. The lines that falls within 10 mm of the left antenna position are shown. The angle between the lines is 0.25°.

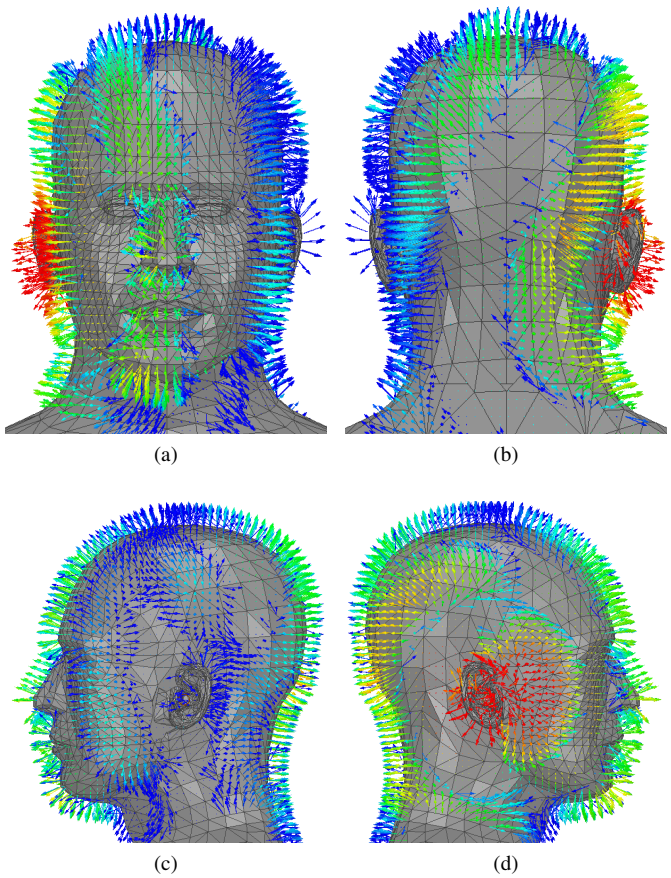

Fig. 4. The SAM phantom head with the simulated electric field just above the surface plotted as vectors seen from the front (a), back (b), left (c), and right (d) side of the head. The logarithmic color scale ranges from 50 V/m (red) to 0.5 V/m (blue).

that the two facets are flattened so they were in the same plane, the geodesic line would simply be a straight line.

When the geodesic lines were found on the original head seen in Fig. 1 the lines had a tendency to group together. There was a large gap between the lines that exit a facet on one or the other edge. This was caused by the large facets. To overcome this, the facet size was reduced. One could say that the head was up-sampled. This was done in the freely available software Blender used for 3D editing. The up-sampling was done with a setting to maintain the total volume. The result can be seen in Fig. 2. It would of course be better to have a mathematical description of the head, that is smooth and differentiable, but it would then be a mathematical challenge in it self to find the geodesic lines. It would be desirable to use the up-sampled head in the simulation, but this creates issues with the meshing of the complex geometry. Here the underlying assumption is that the faceted head does not make a significant difference from a smooth head, neither in simulations nor in the model.

In a few areas the head is concave. This is only in areas in the front of the head, mostly around the nose. The geodesic lines are found as simple straight lines across the concave areas. One could potentially calculate the diffraction at the point where the line escapes the surface of the head and again when it contacts the surface. To reduce the complexity, and on the assumption of low impact on the result, this was not done. Instead, in the calculation of the loss, it has simply been included as a straight piece over the head.

It is noted that when finding the geodesic lines the ears had been removed. The ears are viewed as part of the antenna and the effect from the ears is included in the simulated radiation pattern that is put into the model.

In Fig. 2 geodesic paths originating from the right ears with a length of 200 mm is shown. It is seen that the geodesic lines create a wavefront, **which has travelled 200 mm in the different directions around the head**. The paths around the back and over the top of the head are smoothly distributed. The paths around the front of the head is diffracted in different directions, but they still constitute a relatively uniform wave-front. In Fig. 3 only the geodesic lines that reach the antenna

0018-926X (c) 2018 IEEE. Personal use is permitted, but republication/redistribution requires IEEE permission. See http://www.ieee.org/publications_standards/publications/rights/index.html for more information.

This article has been accepted for publication in a future issue of this journal, but has not been fully edited. Content may change prior to final publication. Citation information: DOI 10.1109/TAP.2018.2882587, IEEE Transactions on Antennas and Propagation

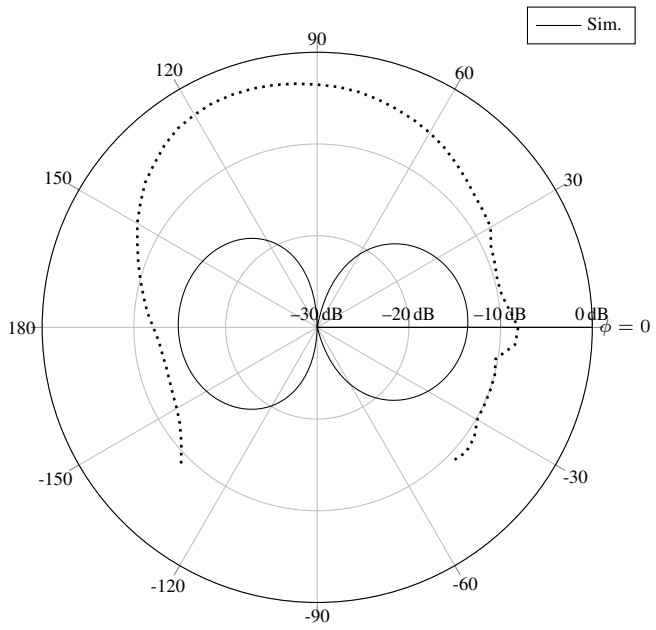

Fig. 5. Plane cut in the XY-plane of the magnitude of the theta component of the simulated radiation pattern at 2.45 GHz (solid line). The dotted line shows the contour of the head.

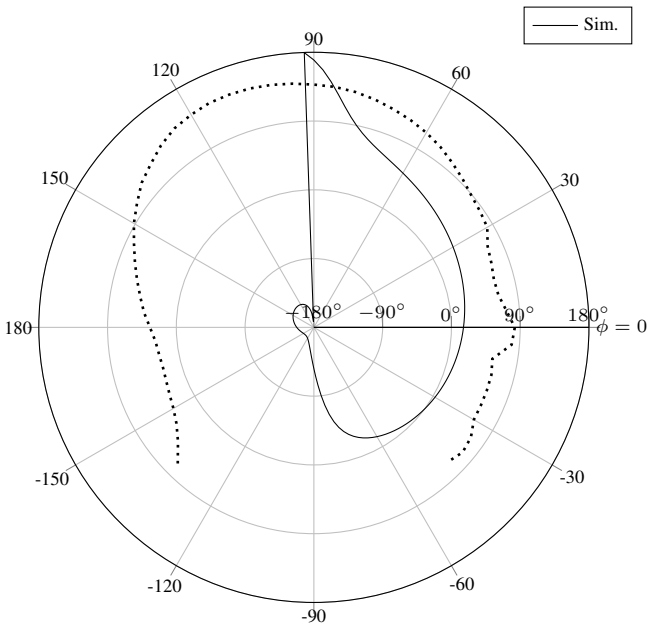

Fig. 6. Plane cut in the XY-plane of the phase of the theta component of the simulated radiation pattern at 2.45 GHz (solid line). The dotted line shows the contour of the head.

on the opposite side of the head are shown. **These were found by extending the lines from Fig. 2 until they pass the point of closest proximity to the left antenna. The lines that, at the closest point, are within 10 mm of the left antenna have been included.** It is clear that there is one path around the back, one over the top and four paths around the front. The four paths in the front run over the tip of the nose, the mouth, the chin and the transition from the head to the neck. There is possibly a path in the front at the root of the nose, but since it is so small the discrete number of lines does not capture it. This also means that it will not have a significant contribution. It is noted that each of the paths either constitute a local minimum or maximum with respect to the path length.

Each of the paths are approximated by 100 points. These are uniformly distributed along the path. To get estimates of the curvature and the torsion, the 100 points are smoothed. This is done with a local regression with a second degree polynomial. For each of these 100 points the attenuation is found. The numerical integration of the total loss is done with the trapezoidal method over the 100 points.

The final numerical challenge is to approximate the derivative $\frac{\mathrm{d}\psi_0}{\mathrm{d}\chi}$. Since the head model is faceted, the distance between lines is not continuous. Therefore the derivative for each of the six paths have been approximated as:

$$\frac{\mathrm{d}\psi_0}{\mathrm{d}\chi} = \sqrt{\frac{\Delta\psi_0 n_{\mathrm{lim}}}{2\chi_{\mathrm{lim}}}} \tag{10}$$

where $\Delta\psi_0 = 0.25°$ is the discrete angle between adjacent lines at the source and n_{lim} is the number of lines for a given path that get within a certain distance, $\chi_{\mathrm{lim}} = 10\,\mathrm{mm}$ of the observation point.

V. Results and Discussion

Various simulations were run to compare with the model. First, the antenna presented in [14] was simulated at 2.45 GHz. In [14] the measurements of the prototype antennas are found. In Fig. 4 the electric field vectors just above the surface of the head is shown. It is clearly seen that wavefronts similar to those in Fig. 2 are present. It is also seen from Fig. 4d that the wavefronts launched from the source have different phases. This justifies the use of the phase of the electric fields in the model. In Fig. 5 the magnitude of the gain of the right antenna in the XY-plane is seen. The antenna has two lobes, one towards the front and one towards the back. In Fig. 6 the phase of the antenna is seen. Compared to Fig. 4d it is seen to explain the phase differences between the lobes.

A simulation in the frequency range of 2 GHz to 3 GHz was done. The gain and phase of the antennas were exported and applied to the model. In Fig. 7 the magnitude of the simulated and modeled path gain is shown. The general trend of the curves are clearly the same; the path gains stay within 6 dB of each other over the entire frequency span. It is noted that even though strict convergence criteria were used, the convergence far away from the resonance frequency of the antenna and below –100 dB can not be completely guaranteed. Small changes in the mesh setup can change the simulation results with a few decibels at the edges of the frequency range, whereas the level at 2.45 GHz stays within 1 dB. In Fig. 8 the phase of the simulated and modeled path gain is shown. Good correspondence between the simulated and modeled results are seen here as well. The difference is again more pronounced at the edges of the frequency range.

To investigate if the common trends of the path gains are only caused by the effect of the reflection coefficient, the MAPG as given by Equation 9 was calculated. The simulated

0018-926X (c) 2018 IEEE. Personal use is permitted, but republication/redistribution requires IEEE permission. See http://www.ieee.org/publications_standards/publications/rights/index.html for more information.

This article has been accepted for publication in a future issue of this journal, but has not been fully edited. Content may change prior to final publication. Citation information: DOI 10.1109/TAP.2018.2882587, IEEE Transactions on Antennas and Propagation

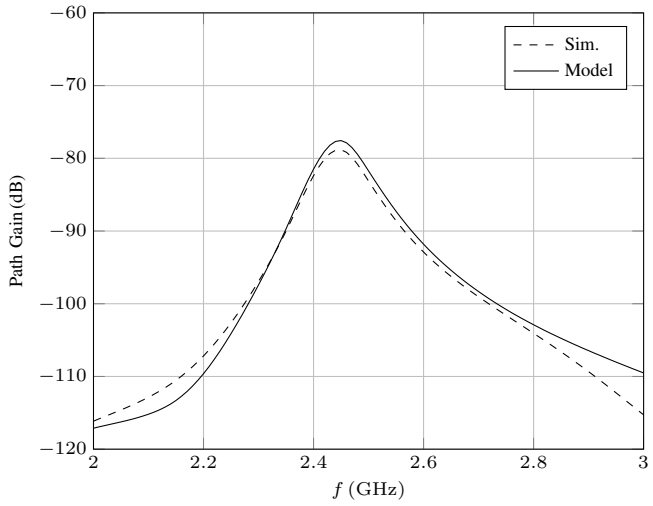

Fig. 7. Simulated (dashed line) and modeled (solid line) E2E path gain.

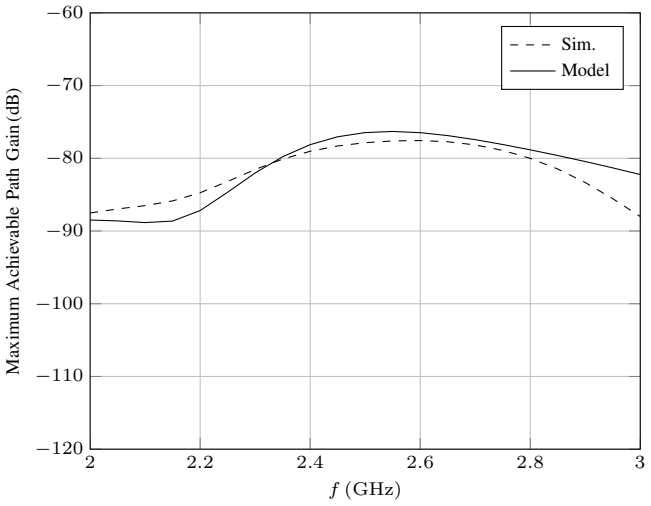

Fig. 9. Simulated (dashed line) and modeled (solid line) E2E maximum achievable path gain.

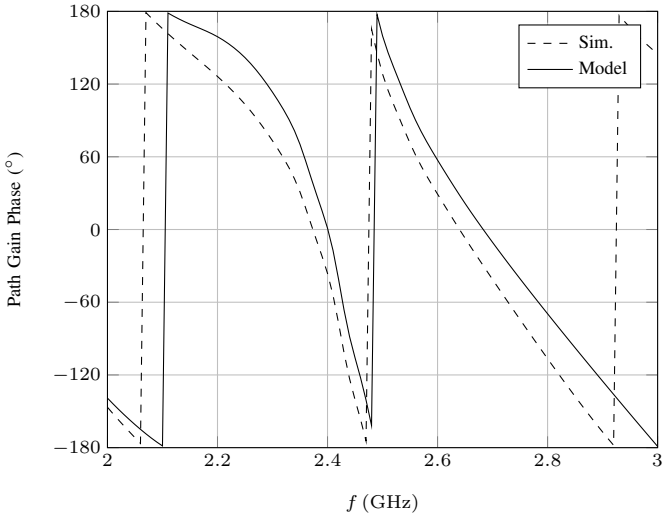

Fig. 8. Simulated (dashed line) and modeled (solid line) phase of the E2E path gain.

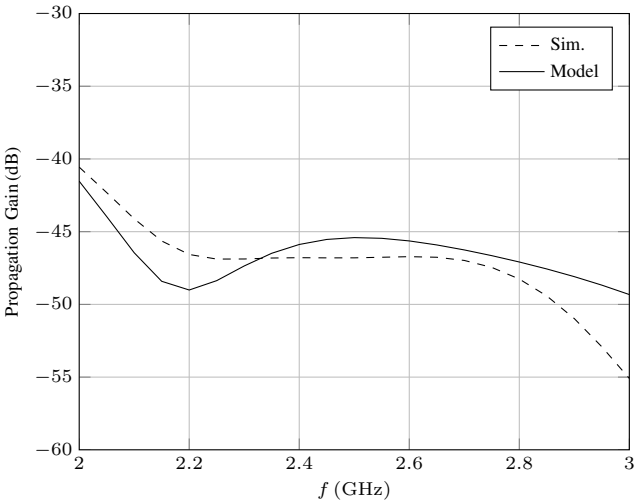

Fig. 10. Simulated (dashed line) and modeled (solid line) E2E propagation gain.

and modeled MAPG is shown in Fig. 9. It is seen that the trends of the two path gains remain the same even without the **"windowing"** effect of the reflection coefficient, **which has been removed by Equation 9**. Similarly, in order to see if the effect of the efficiency is the cause of the trend of the MAPG, the propagation gain, S_{21}^{prop}, was calculated. The propagation gain is given as the maximum achievable path gain divided by the radiation efficiency, e_{cd}, squared:

$$S_{21}^{\mathrm{prop}} = \frac{|S_{21}^{\mathrm{max}}|}{e_{\mathrm{cd}}^2} \tag{11}$$

The radiation efficiency is squared to remove the effect from the transmitting and the receiving antenna. The propagation gain is shown in Fig. 10. Even though the differences between the simulated and modeled result are seen more clearly here, the general trend remains the same.

The contribution of the different paths around the head to the total modeled MAPG is seen in Fig. 11. The four paths around the front of the head have been aggregated. The main contributions clearly come from the front and back path. It is seen that the destructive interference of these two paths is the cause of the dip in the propagation gain around 2.2 GHz. The MAPG of both the front and the back path alone is higher than the total MAPG. The two paths are also seen to have increasing destructive interference towards 3 GHz since both path MAPGs are getting close to the total MAPG.

Here the modeled results use the radiation pattern from a full E2E simulation with a radiation surface defined around the ear and transformed to the far-field. An additional simulation was done where only a small rectangular cut-out including the right ear with the antenna inside was included. If the radiation pattern from that simulation is used, the modeled results remain the same within less than 1 dB. This enables the use of the model where only a cut-out simulation has been made. This is a much simpler and faster simulation to do than the full E2E simulation.

Another set of simulations were done at 2.45 GHz. The

0018-926X (c) 2018 IEEE. Personal use is permitted, but republication/redistribution requires IEEE permission. See http://www.ieee.org/publications_standards/publications/rights/index.html for more information.

This article has been accepted for publication in a future issue of this journal, but has not been fully edited. Content may change prior to final publication. Citation information: DOI 10.1109/TAP.2018.2882587, IEEE Transactions on Antennas and Propagation

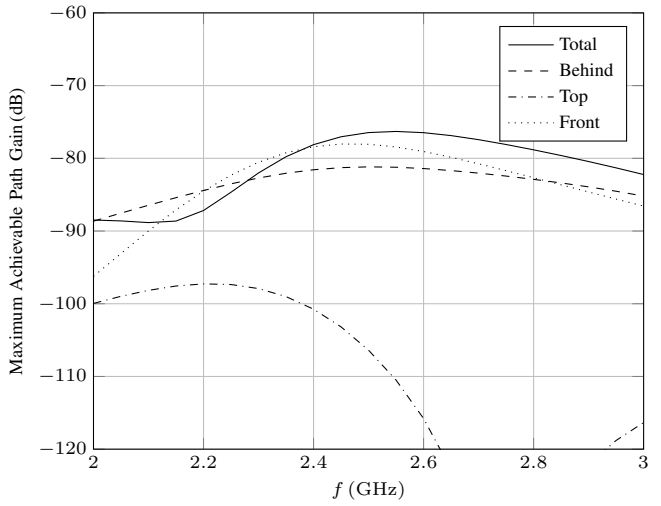

Fig. 11. Modeled E2E maximum achievable path gain divided into different paths. Total (solid), behind the head (dashed), over the top of the head (dash-dotted), and around the front of the head (dotted).

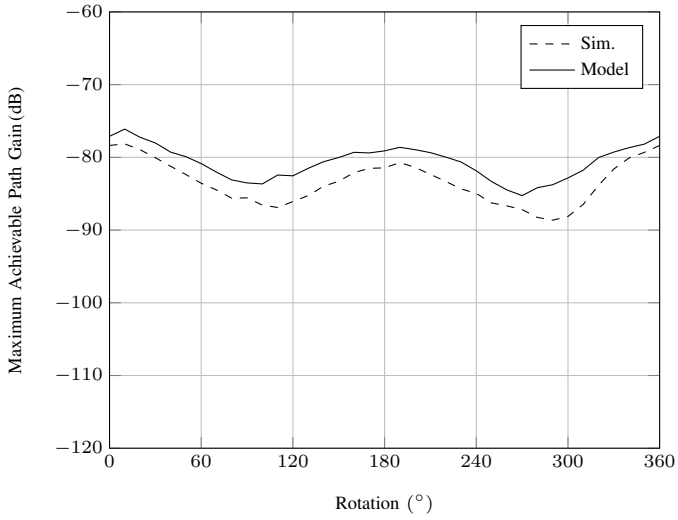

Fig. 12. Simulated (dashed line) and modeled (solid line) E2E maximum achievable path gain for different angles of rotation of the antenna.

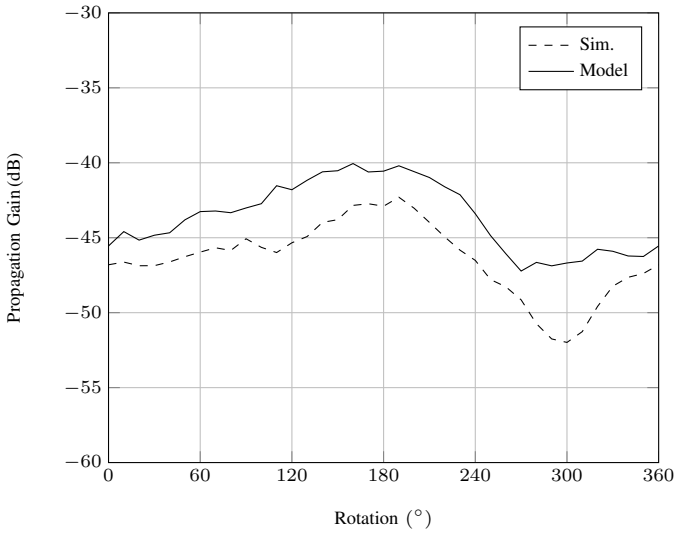

Fig. 13. Simulated (dashed line) and modeled (solid line) E2E propagation gain for different angles of rotation of the antenna.

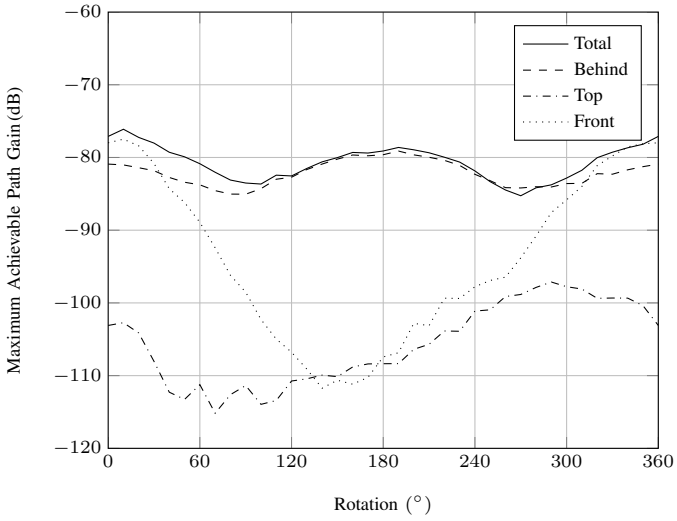

Fig. 14. Modeled E2E maximum achievable path gain divided into different paths for different angles of rotation of the antenna. Total (solid), behind the head (dashed), over the top of the head (dash-dotted), and around the front of the head (dotted).

antenna was rotated in the ear in steps of 10° as done in [17]. Measurements can be found in that article as well. The simulated and modeled MAPG can be seen in Fig. 12. It is clear that the simulated and modeled results correlate well. The simulated and modeled propagation gain is seen in Fig. 13. The trends are still the same although the model does not replicate the entire dip in propagation gain at 300°.

In Fig. 14 the contributions of the different paths to the total MAPG is shown. At around 0° the main contribution comes from the front path. At around 180° almost no energy comes from the front path. The total MAPG is made up almost entirely of the back path contribution. This change in "main" path is not seen in Fig. 12, which confirms that the model captures the E2E propagations correctly.

VI. Conclusion

The first E2E propagation model to use the geodesic lines around a head has been presented. Furthermore, it is the first E2E model to utilize a lossy dielectric GTD approximation. The model shows good correlation with simulation, especially at the resonance frequency of the antenna. The correlation remains visible even when the envelope effect of the reflection coefficient as well as the efficiency is removed. Simulation of a small cut-out box around the ear combined with the model enables faster results for the E2E path gain. It has been shown that the model captures the transition between different 'main' paths. This validates the model's assumption of the division of the propagation into the different geodesic paths around the head.

0018-926X (c) 2018 IEEE. Personal use is permitted, but republication/redistribution requires IEEE permission. See http://www.ieee.org/publications_standards/publications/rights/index.html for more information.

This article has been accepted for publication in a future issue of this journal, but has not been fully edited. Content may change prior to final publication. Citation information: DOI 10.1109/TAP.2018.2882587, IEEE Transactions on Antennas and Propagation

REFERENCES

[1] N. P. B. Kammersgaard, S. H. Kvist, J. Thaysen, and K. B. Jakobsen, "Off-body transmission range improvement for hearing instruments by the use of ear-to-ear communication," in *Proceedings of 2015 Loughborough Antennas & Propagation Conference*. IEEE, 2015.

[2] T. E. P. Alves, B. Poussot, and J.-M. Laheurte, "Analytical Propagation Modeling of BAN Channels Based on the Creeping-Wave Theory," *IEEE Trans. Antennas Propagat.*, vol. 59, no. 4, pp. 1269–1274, Apr 2011.

[3] C. Oliveira and L. M. Correia, "A Statistical Model to Characterize User Influence in Body Area Networks," in *Vehicular Technology Conference Fall (VTC 2010-Fall), 2010 IEEE 72nd*, Sep 2010.

[4] E. Plouhinec, B. Uguen, M. Mhedhbi, and S. Avrillon, "3D UTD modeling of a measured antenna disturbed by a dielectric circular cylinder in WBAN context," in *2014 IEEE 79th Vehicular Technology Conference (VTC Spring)*, May 2014, pp. 1–5.

[5] M. Ghaddar, L. Talbi, and T. A. Denidni, "Human Body Modelling for Prediction of Effect of People on Indoor Propagation Channel," *Electronics Letters*, vol. 40, no. 25, pp. 1592–1594, Dec 2004.

[6] R. Chandra and A. J. Johansson, "An Analytical Link-Loss Model for On-Body Propagation Around the Body Based on Elliptical Approximation of the Torso With Arms' Influence Included," *IEEE Antennas Wirel. Propag. Lett.*, vol. 12, pp. 528–531, Apr 2013.

[7] Y. Zhao, Y. Hao, A. Alomainy, and C. G. Parini, "UWB On-Body Radio Channel Modeling Using Ray Theory and Subband FDTD Method," *IEEE Trans. Microwave Theory Tech.*, vol. 54, no. 4, pp. 1827–1835, Apr 2006.

[8] Y. Hao, A. Alomainy, Y. Zhao, C. G. Parini, Y. I. Nechayev, P. S. Hall, and C. C. Constantinou, "Statistical and Deterministic Modelling of Radio Propagation Channels in WBAN at 2.45GHz," in *Antennas and Propagation Society International Symposium 2006, IEEE*, 2006, pp. 2169–2172.

[9] S. H. Kvist, J. Thaysen, and K. B. Jakobsen, "Ear-to-ear on-body channel model for hearing aid applications," *IEEE Transactions on Antennas and Propagation*, vol. 63, no. 1, pp. 344–352, 2015.

[10] R. Chandra and A. J. Johansson, "A link loss model for the on-body propagation channel for binaural hearing aids," *IEEE Trans. Antennas Propagat.*, vol. 61, no. 12, pp. 6180–6190, 2013.

[11] N. P. B. Kammersgaard, S. H. Kvist, J. Thaysen, and K. B. Jakobsen, "Validity of PEC approximation for on-body propagation," *2016 10th European Conference on Antennas and Propagation (EuCAP)*, 2016.

[12] ——, "Geometrical theory of diffraction formulation for on-body propagation," *Submitted to IEEE Transactions on Antennas and Propagation*, 2018.

[13] J. Vidkjaer, "Linear Active Two-Ports," in *Class Notes, 31415 RF-Communication Circuits*, 2013, ch. 3. [Online]. Available: http://rftoolbox.dtu.dk/book/Ch3.pdf

[14] N. P. I. Kammersgaard, S. H. Kvist, J. Thaysen, and K. B. Jakobsen, "In-the-ear circular-shaped balanced inverted-a antenna for hearing instruments," *IEEE Antennas and Wireless Propagation Letters*, vol. 15, pp. 1839–1843, 2016.

[15] "IEEE recommended practice for determining the peak spatial-average specific absorption rate (SAR) in the human head from wireless communications devices: Measurement techniques," 2013.

[16] A. Pressley, *Elementary differential geometry*, 2nd ed. Springer, 2010.

[17] N. P. I. Kammersgaard, S. H. Kvist, J. Thaysen, and K. B. Jakobsen, "Impact of placement of in-the-ear antenna on ear-to-ear path gain," *Proceedings of 2015 Loughborough Antennas & Propagation Conference*, 2015.

Nikolaj Peter Brunvoll Kammersgaard received the B.Sc. and M.Sc. degrees in electrical engineering from the Technical University of Denmark, Lyngby, in 2013 and 2014, respectively. Since 2014, he has been affiliated with GN Hearing A/S, a Danish hearing aid manufacturer, where he is currently pursuing an Industrial Ph.D. degree in cooperation with the Technical University of Denmark. His research interests include on-body antennas and propagation, as well as electrically small antennas and physical limitations of antennas. He was awarded the Student Paper Award for best student paper at the International Workshop on Antenna Technology 2015. In 2015, he was awarded with "Kandidatprisen" from the Danish Association of Engineers (IDA). The award is given to three recently graduated promising electrical engineers for their Master's thesis.

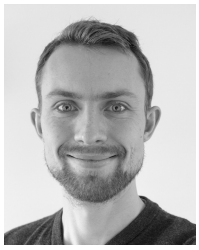

Søren Helstrup Kvist received the B.Sc., M.Sc. and Ph.D. degrees in electrical engineering from the Technical University of Denmark in 2007, 2009 and 2014, respectively. Since 2009 he has been affiliated with GN Hearing A/S, a Danish hearing aid manufacturer, where he is currently employed as manager of the Radio Systems group. His research interests include on-body antennas and propagation, as well as electrically small antennas and physical limitations of antennas. Dr. Kvist was awarded the "Elektroprisen 2015" from the Danish Association of Engineers (IDA). The award is given for excellent technical and scientific work within electrical engineering.

Jesper Thaysen received the B.Sc., M.Sc. and Ph.D. degrees in electrical engineering from the Technical University of Denmark in 1998, 2000 and 2005, respectively, and an MBA from Middlesex University in 2015. Since 2008 he has been employed at GN Hearing A/S, a Danish hearing aid manufacturer, where he currently acts as the Head of the Global Manufacturing Organization. His research interests include small antennas and on-body antennas and propagation. Dr. Thaysen has overseen more than 40 B.Sc. and M.Sc. students, as well as 3 Ph.D. students, as the company representative in university-industry cooperative projects.

Kaj Bjarne Jakobsen received the B.Sc.EE and the M.Sc.EE degree from the Technical University of Denmark, Kgs. Lyngby, in 1985 and 1986, respectively, the Ph.D. degree in Electrical Engineering from University of Dayton, Dayton, OH, in 1989, and the HD in Organization and Management, Copenhagen Business School, Copenhagen in 2000. From 1986-1989 he was a Fulbright Scholar at the Department of Electrical Engineering, University of Dayton, OH. Since 1990 he has been with the Department of Electrical Engineering, Technical University of Denmark, Kgs. Lyngby, where he is Associate Professor. His research interests are in body-centric wireless network, wireless body area network, and body sensor network. He received in 1989 the NCR Stakeholder Award, Ohio, USA, and was appointed Teacher-of-the-Year at the Technical University of Denmark in 1994.

0018-926X (c) 2018 IEEE. Personal use is permitted, but republication/redistribution requires IEEE permission. See http://www.ieee.org/publications_standards/publications/rights/index.html for more information.